

Capillary microreactor with PdZn/(Ti, Ce)O₂ coating for selective hydrogenation of 2-methyl-3-butyn-2-ol



Lyudmila B. Okhlopkova ^{a,*}, Igor P. Prosvirin ^{a,b}, Mikhail A. Kerzhentsev ^a, Zinfer R. Ismagilov ^{a,c}

^a Boreskov Institute of Catalysis, SB RAS, Lavrentieva Ave. 5, Novosibirsk, 630090, Russia

^b Novosibirsk State University, Pirogova St.2, Novosibirsk, 630090, Russia

^c Federal Research Center of Coal and Coal-Chemistry, SB RAS, Sovetsky Ave. 18, Kemerovo, 650000, Russia

ARTICLE INFO

Keywords:

Capillary microreactor
Ce-doped titania
Palladium nanoparticles
Selective hydrogenation
2-Methyl-3-butyn-2-ol

ABSTRACT

The catalytic properties of Pd/Ti_{0.95}Ce_{0.05}O₂, Pd₈₀Zn₂₀/Ti_{0.95}Ce_{0.05}O₂ and Pd/TiO₂ coatings on the inner wall of capillary microreactor were studied in the selective hydrogenation of 2-methyl-3-butyn-2-ol (MBY). The effect of initial MBY concentration, hydrogen partial pressure, reaction temperature on activity and selectivity to MBE was studied for three microcapillaries coated with different catalysts. The most noticeable impact was observed for the catalyst composition such as Ce-doping and Zn addition to Pd nanoparticles and can be explained by the different strengths of MBY adsorption. The catalyst activity increases in the series: Pd/TiO₂ < Pd₈₀Zn₂₀/Ti_{0.95}Ce_{0.05}O₂ < Pd/Ti_{0.95}Ce_{0.05}O₂, while the adsorption constant of MBY and selectivity to 2-methyl-3-butyn-2-ol (MBE) decline. The catalytic performance also depends on test duration and oxidation-reduction treatments. The highest yield of MBE (95.8 %) at 99 % conversion on Ce-doped coatings was obtained on Pd₅₀Zn₅₀/Ti_{0.95}Ce_{0.05}O₂ coating after 68 h on stream.

1. Introduction

Selective hydrogenation of alkyne alcohol represents a crucial stage in many fine chemical processes since the semihydrogenated alkene alcohols are widely used in the fragrance production and pharmaceuticals. In the study of selective hydrogenation, 2-methyl-3-butyn-2-ol (MBY) is considered to be the starting material in DSM Nutritional Products [1]. Slurry-type reactors are most often used in industry as batch or semi-continuous reactors [2]. Slurry-type reactors have several disadvantages that limit their use in some processes. In the case of a stirred tank reactor, the catalyst separation step is difficult due to catalyst abrasion and the conversion, and selectivity in a continuously operated slurry bubble column also decreases due to back mixing. Another important disadvantage of conventional reactors for multiphase reactions in pilot and industrial plants is the low rate of mass and heat transfer. These disadvantages found in conventional multiphase systems result in increased development time, high operating costs and low productivity. The fundamental difference between microstructured

(capillary) reactors and standard volumetric ones is the laminar flow of fluids (liquids and gases). The use of capillaries provides almost perfect mixing of reagents due to diffusion. Ideal diffusion mixing pre-determines the high selectivity and purity of the reaction, and, as a consequence, a significant reduction in the formation of by-products and intermediate products [3]. The ratio of the contact area to the volume of the reaction mixture of microreactors is many times greater than the contact area in bulk reactors [4]. The most efficient heat exchange allows for instant heating and cooling of the reaction mixtures, maintaining isothermal reaction conditions at all points in the system. The micro-sizes of the capillaries allow the use of such reactors for operation under high pressure. All of the above factors - contact area, heat exchange, temperature, pressure - determine the kinetics of reactions. The advantages of microstructure reactors lead to a significant reduction in reaction times, ultimately predetermining higher productivity of continuous flow reactors compared to traditional bulk reactors. One of the decisive aspects of modern chemistry is the safety of reactions and processes. It is easy to calculate that with an equal amount of starting

Abbreviations: MBY, 2-methyl-3-butyn-2-ol; MBE, 2-methyl-3-butyn-2-ol; MBA, 2-methyl-2-butanol.

* Corresponding author.

E-mail addresses: lokhlopkova@yandex.ru, mila65@catalysis.ru (L.B. Okhlopkova).

<https://doi.org/10.1016/j.cep.2020.108240>

Received 2 September 2020; Received in revised form 1 November 2020; Accepted 24 November 2020

Available online 27 November 2020

0255-2701/© 2020 Elsevier B.V. All rights reserved.

materials and final product and the same productivity, the volume of the reaction mixture in a batch reactor is several orders of magnitude higher than in a flow reactor [5]. The minimum amount of the reaction mixture in the reactor minimizes the explosion hazard of exothermic reactions. In addition to process safety, a significant reduction in the amount of reagents plays a significant role in solving environmental concerns [6]. More accurate control of reactions in a continuous flow mode minimizes the amount of by-products. One of the key advantages of continuous flow reactor technology is the accuracy of scaling and numbering. Due to the high speed and precision of changing the reaction parameters (temperature, pressure, flow rates, reagent ratio, use of catalysts, etc.) microreactor systems are an ideal tool for efficient and fast optimization of reactions [7].

Microfluidic technologies have been recently proposed to improve the fine chemistry processes. Selective hydrogenation of MBY in methanol has been previously studied in the capillary microreactors with diameter 220 μm the inner surface of which was covered with Pd₂₅Zn₇₅/TiO₂ and Pd/TiO₂ [8]. Capillary microreactors allowed overcoming the mass transfer limitation and to improve the selectivity to the desired product by precise control of the liquid residence time [9–12]. To perform hydrogenations in a microreactor, titania films can be recently prepared via evaporation induced self-assembly [8,9]. A limitation of the use of pure titanium dioxide materials is that they are very sensitive to moisture and have poor thermal stability at high pre-treatment temperatures. This drawback does not exist in the case of multicrystalline, mesoporous ordered materials [13]. Recently, the use of mixed metal oxide systems has been highlighted to improve the stability and/or surface properties of mesoporous oxides [14–16]. When using Ce-doped coatings, the shortcomings of titanium systems can be overcome due to the increased chemical and thermal stability of the coating [17]. In this article we present the continuous selective hydrogenation of MBY in capillary microreactors to provide greater control over the chemical process than classical batch and semi-continuous technologies and to improve the environmental performance of the process. The reaction was optimized with respect of the activity, selectivity to 2-methyl-3-butene-2-ol (MBE) and stability for one of the three catalysts Pd/Ti_{0.95}Ce_{0.05}O₂, Pd₈₀Zn₂₀/Ti_{0.95}Ce_{0.05}O₂, Pd/TiO₂. Pd was chosen for its high activity. Secondary metals are often included in a catalyst to increase the selectivity to MBE [18–21]. Recent studies have analyzed the possibility of using intermetallic PdZn nanoparticles with electronic properties different from those of the parent Pd metal [8,9,22,23].

2. Materials and methods

2.1. Preparation of the catalytic capillaries

Four capillary reactors were coated with a catalytic layer. Three of them with a diameter of 220 μm were supplied by SGE (product number 062463 [24]) and one with a diameter of 530 μm was supplied by AGILENT (product number 160-2530-10 [25]). Each capillary was made from polyimide coated fused silica with a length of 10 m, which was pretreated with 1 M NaOH solution at a temperature of 313 K for 1 h. Then the capillary was alternately washed with water and ethanol at a temperature of about 298 K and dried at 373 K for 12 h in an oven. The coatings were synthesized by the sol-gel method using a colloidal solution of nanoparticles according to the previously described procedure [26,27]. Colloidal Pd and PdZn nanoparticles were prepared by solvent reduction with a poly-N-vinylpyrrolidone/metal molar ratio 10/1 as described in previous work [28]. Part of the sol was used to dip-coat the inner wall of fused silica capillaries at a rate of 1 cm/s in an argon atmosphere. The capillaries, as well as the other part of the sol, were kept in a glove box for 24 h at a relative humidity of 80 %, followed by calcination at 573 K under a pressure of 13 mbar for 2 h with a heating rate of 1 K/min. The four coatings described above had the following catalyst loadings with a nominal nanoparticle loading:

Pd/Ti_{0.95}Ce_{0.05}O₂ – 0.7 wt.% Pd on 0.28 mg of Ti_{0.95}Ce_{0.05}O₂; Pd₈₀Zn₂₀/Ti_{0.95}Ce_{0.05}O₂ – 0.87 wt.% Pd₈₀Zn₂₀ on 0.35 mg of Ti_{0.95}Ce_{0.05}O₂; Pd/TiO₂ – 0.93 wt.% Pd on 0.42 mg of TiO₂; Pd₅₀Zn₅₀/Ti_{0.95}Ce_{0.05}O₂ – 0.89 wt.% Pd₅₀Zn₅₀ on 2.5 mg of Ti_{0.95}Ce_{0.05}O₂. It should be noted that in the latter case, the mass of the oxide is 7 times greater than that of a similar sample deposited on a capillary with a smaller diameter. For samples deposited on a capillary with a 530 mm in diameter, not only the area of the coating increases but also its thickness [29]. Calculations have shown that with an increase in the capillary diameter from 220 to 530 mm, the coating volume increases by a factor of 7.

The coating Pd₅₀Zn₅₀/Ti_{0.95}Ce_{0.05}O₂ on the inner surface of capillary with diameter of 530 μm was treated under different conditions, the number indicates activation treatment: 1) 138 h in a continuous flow of the reaction solution and hydrogen; 2) reduction of sample No. 1 in hydrogen flow at 573 K for 2 h; 3) calcination of sample No. 2 at 573 K for 2 h with the subsequent reduction in hydrogen flow at 573 K for 2 h; 4) calcination of sample No. 3 at 673 K for 2 h with subsequent reduction in hydrogen flow at 573 K for 2 h; 5) reduction of sample No. 4 in hydrogen flow at 573 K for 2 h.

2.2. Hydrogenation experiments

2.2.1. Batch reactor

The hydrogenation experiments were conducted using an autoclave reactor with a total volume of 130 mL. Prior to use, the powder samples were ground in a mortar, introduced into the reactor, purged with argon, hydrogen was injected under a pressure of up to 10 atm, heated to 523 K and held for 2 h. After activation, the reactor was cooled to room temperature. 0.1 M MBY and 0.1 M 1-butanol in methanol (50 mL) was purged in argon, transferred to the reactor, the hydrogen pressure was increased to 5 atm, heated to 333 K, and held at this temperature for 30 min. The hydrogenation reaction started after stirring at 2000 rpm. The analysis of the reaction mixture was performed offline using an Agilent 7890A gas chromatograph equipped with an HP-5 capillary column (diameter: 0.32 mm, length: 30 m) and an FID (flame ionization detector) detector. 1-butanol was used as an internal standard.

2.2.2. Continuous capillary reactor

The coatings on the inner surface of the silica capillary were tested in the setup presented in Fig. 1 at the temperature range from 303 to 333 K. The setup consisted of a continuous flow syringe pump, hydrogen and helium mass flow controllers, connected to the reactor by tubes (250 μm in diameter) and thermostatic oven. The coating on the inner surface of the silica capillary was preliminarily washed by withdrawing 50 mL of methanol and reduced with hydrogen at 573 K. A gas consisting of a hydrogen/helium mixture and a solution of MBY and 1-butanol in methanol were mixed in a T-mixer. Five reaction parameters were varied: MBY concentration between 0.04 and 0.3 M, H₂ partial pressure from 0.3 to 1, liquid flow between 5 and 60 $\mu\text{L}/\text{min}$, the H₂/He flow between 0.1 and 4.0 mL/min (STP), temperature from 303 to 333 K. The MBY solution and hydrogen were continuously flowing through the reactor within 10–30 min, then 3 liquid samples were collected, diluted 3:1 with methanol and analyzed using a gas chromatograph Crystall 2000 M equipped with an SKTFT-50X capillary column (diameter: 0.22 mm, length: 30 m) and a FID detector. MBY conversion was defined as $X = \frac{(C_{MBY,0} - C_{MBY})}{C_{MBY,0}} \times 100$; selectivity was defined as $S_{MBE} = \frac{C_{MBE}}{(C_{MBY,0} - C_{MBY})} \times 100$; activity in a batch reactor was defined as $A = \frac{(C_{MBY,0} - C_{MBY}) \times V}{t \times molPd} \times 100$; activity in microcapillary reactor was defined as $A = \frac{(C_{MBY,0} - C_{MBY}) \times v_l}{molPd} \times 100$; yield of MBE was defined as $Y = \frac{C_{MBE}}{C_{MBY,0}} \times 100$; where $C_{MBY,0}$ is the initial concentration of MBY; C_{MBY} and C_{MBE} are current concentrations of MBY and MBE, respectively; V is the reaction volume; v_l liquid flow rate, t is the current reaction time in

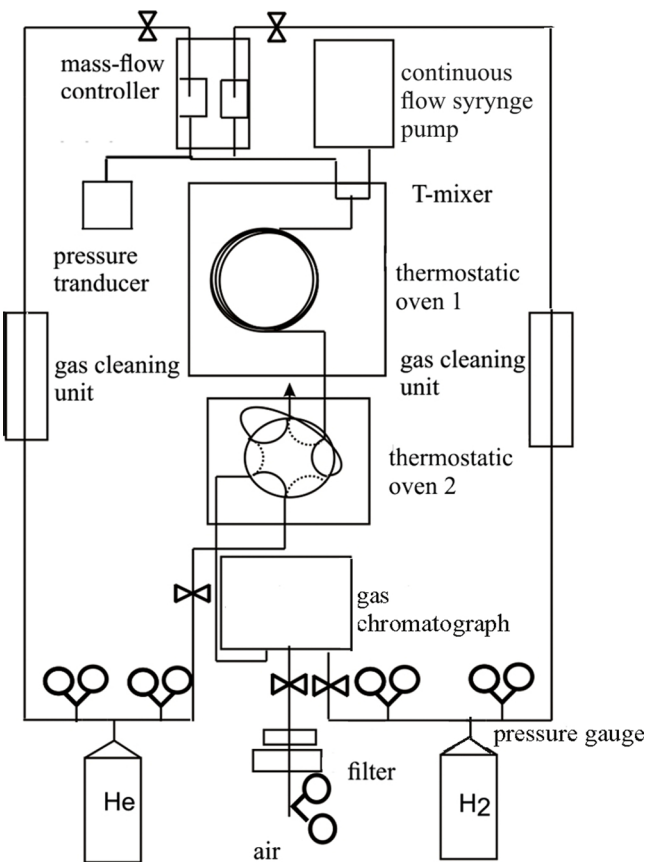


Fig. 1. System for continuous flow hydrogenation in a capillary reactor.

the autoclave.

3. Results

3.1. Effect of reactor type

The performance of a microcapillary reactor was compared to that of a batch type reactor (Table 1). A significant difference was obtained in the selectivity. Higher selectivity in the microcapillary reactor can be achieved through precise control of the reagent residence time. An increase in the residence time results in a loss of selectivity due to the complete hydrogenation of the MBE. Selectivity to MBE at 86 % conversion decreased from 91 % to 79 % with a decrease in the H₂ flow rate

Table 1

Effect of catalyst and reactor type on the activity at 20 % conversion and selectivity at 50 % and 96 % conversion in the hydrogenation of 2-methyl-3-butyn-2-ol.

Sample	Reactor	Activity, molMBY/molPd/s	S ₅₀ , %	S ₉₆ , %	Maximum MBE yield, %
Pd/Ti _{0.95} Ce _{0.05} O ₂	microreactor	2.5 ^a	88.2	86.3	82.8
Pd/Ti _{0.95} Ce _{0.05} O ₂	microreactor	1.7 ^b	87	79 ^b	–
Pd/Ti _{0.95} Ce _{0.05} O ₂	microreactor	4.4 ^c	93	91 ^b	–
Pd/Ti _{0.80} Ce _{0.20} O ₂	batch	6.3 ^d	–	67.0	65.0
Pd ₈₀ Zn ₂₀ /Ti _{0.95} Ce _{0.05} O ₂	microreactor	2.3 ^a	96.8	92.7	89.0
Pd ₈₀ Zn ₂₀ /Ti _{0.95} Ce _{0.05} O ₂	batch	3.3 ^d	92.0	79.7	81.3
Pd ₅₀ Zn ₅₀ /Ti _{0.95} Ce _{0.05} O ₂	microreactor	2.0 ^d	98.9	94.5	90.7
Pd/TiO ₂	microreactor	0.96 ^a	98.9	93.9	90.1
Pd/TiO ₂	batch	2.6 ^e	90.7	77.2	74.4
Pd + Pd/CaCO ₃	batch ^f	0.04	–	–	94.5

^a Reaction conditions: MBY 0.2 M, v_g– 2.00 mL/min, 1 atm of H₂, T 313 K.

^b Reaction conditions: MBY 0.2 M, v_g– 1.00 mL/min, 1 atm of H₂, T 313 K. Selectivity at 86 % conversion.

^c Reaction conditions: MBY 0.2 M, v_g– 4.00 mL/min, 1 atm of H₂, T 313 K.

^d Reaction conditions: MBY 1 M, v_g– 6.00 mL/min, 1 atm of H₂, T 313 K.

^e Reaction conditions: MBY:Pd = 6000, 50 mL of methanol, 5 atm of H₂, T 333 K.

^f Reaction conditions: MBY:Pd = 2400, 200 mL of H₂O, 5 atm of H₂, T 308 K [35].

from 4 ml/min to 1 ml/min. The hydrogen flow rate was 25 times greater than the liquid velocity, providing a 5:1 M ratio of hydrogen to the substrate and full hydrogenation even at lower gas flow rates. Gas and liquid flow rates have the main effect on the structure of the two-phase flow, setting the flow regime (slug flow and annular flow). For round pipes, it is advisable to use the ratios of inertial and capillary forces in the form of Weber numbers calculated from the superficial velocities of gas and liquid [30]. The Weber number is defined as:

$$W_e = \frac{U^2 \times d_{eq} \times \rho_L}{\sigma}$$

where U is the superficial velocity, d_{eq} is the equivalent channel diameter, ρ_L is the liquid density, and σ is the surface tension. The annular flow zone can be represented by the following expressions:

$$W_{eGS} \geq 11.0 \times W_{LS}^{0.14}$$

$$W_{eLS} \leq 3.0$$

At a low gas flow rate (1 ml/min), the value of W_{eGS} (13) exceeds the value of 11.0 × W_{LS}^{0.14} (8.5), even at a high liquid flow rate (40 μL/min). The range of the applied gas and liquid flow rates corresponds to the annular flow regime. As a result of the decreased ratio between the gas and liquid flow rates, the liquid film flowing along the channel walls becomes thicker, which results in a longer liquid residence time in the reactor. This decreases the selectivity towards the partially hydrogenated product because at a higher liquid residence time the subsequent hydrogenation of MBE occurs. The selectivity to MBE is higher than that observed in a batch reactor at a hydrogen flow rate of 2 ml/min.

3.2. Activity and selectivity under different conditions

We carried out a study on different variables potentially influencing the conversion and selectivity of MBY reduction. We analyzed the influence of the following factors: the effect of liquid residence time, the presence of Zn, the effect of Ce doping of TiO₂, changes in the initial MBY concentration, hydrogen partial pressure and temperature by comparing Pd/Ti_{0.95}Ce_{0.05}O₂, Pd₈₀Zn₂₀/Ti_{0.95}Ce_{0.05}O₂ and Pd/TiO₂ catalysts. Fig. 2a shows the conversion at a constant temperature of 313 K. The MBY conversion decreases with an increasing flow rate. Fig. 2b shows the corresponding selectivity of each catalyst to MBY and 2-methyl-2-butanol (MBA).

Selectivity versus conversion curves were plotted for all catalysts (Fig. 3) from the data presented in Fig. 2. All catalysts showed constant selectivity with respect to MBE and MBA with a conversion of about 100 %. Differences between the catalysts appeared at a conversion below 50 %. The selectivity to MBE over Pd/Ti_{0.95}Ce_{0.05}O₂ and PdZn/

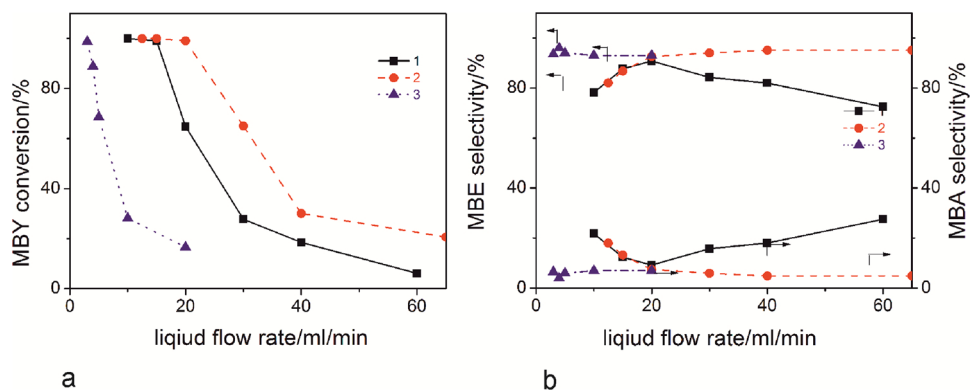


Fig. 2. Effect of liquid flow rate on conversion (a) and selectivity (b) over Pd/Ti_{0.95}Ce_{0.05}O₂ (1), Pd₈₀Zn₂₀/Ti_{0.95}Ce_{0.05}O₂ (2) and Pd/TiO₂ (3). MBY 0.2 M (1,2), 0.11 M (3), v_g- 2.00 mL/min, H₂ 1 atm, T 313 K.

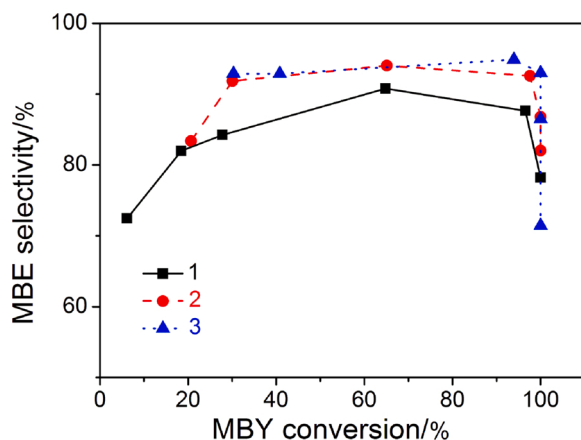


Fig. 3. MBE selectivity as a function of MBY conversion. Pd/Ti_{0.95}Ce_{0.05}O₂ (1), Pd₈₀Zn₂₀/Ti_{0.95}Ce_{0.05}O₂ (2), Pd/TiO₂ (3). v_l- 0.020 mL/min, v_g- 2.00 mL/min, H₂ 1 atm, (1, 2)- MBY 0.2 M, 3 - MBY 0.1 M, T 313 K.

Ti_{0.95}Ce_{0.05}O₂ was lower compared to undoped Pd/TiO₂. As the MBY conversion increases from 50 to 96 % the selectivity to MBE decreases from 88.2 % to 86.3 % over the Pd/Ti_{0.95}Ce_{0.05}O₂, from 96.8 % to 92.7 % over Pd₈₀Zn₂₀/Ti_{0.95}Ce_{0.05}O₂, and from 98.9 % to 93.9 % over Pd/TiO₂ (Table 1). These plots indicate that selectivity depends on catalyst composition. Doping by Ce reduces selectivity, while the addition of Zn to the Pd nanoparticles improves the selectivity to MBE over the doped catalyst, but is still inferior in selectivity to the undoped coating (Fig. 3). Pd₈₀Zn₂₀/Ti_{0.95}Ce_{0.05}O₂ coating represents a compromise between the higher activity that can be achieved on Pd/Ti_{0.95}Ce_{0.05}O₂ catalysts and higher selectivity demonstrated by the Pd/TiO₂ coating. The introduction of a larger amount of zinc to palladium (molar ratio Pd/Zn 1/1) made it possible to increase the selectivity of the process since it was found in [22] that this molar ratio is optimal for achieving high activity and selectivity (Table 1).

Lockhart-Martinelli-Chisholm equation was used to calculate the liquid residence time based on the liquid flow rate [31] (in Supplementary SI3). The catalytic behavior of Pd/Ti_{0.95}Ce_{0.05}O₂, Pd₈₀Zn₂₀/Ti_{0.95}Ce_{0.05}O₂ and Pd/TiO₂ coatings during MBY hydrogenation was compared on Fig. 4a-c. The carbon balance for these systems was 100 ± 2 % (Fig. 4d-f), showing that MBY, MBE and MBA are the main products. It should be noted that the induction period (up to 20 % of MBY conversion) (Fig. 4a-c) is probably associated with the active center formation [32]. In the presence of MBY, full hydrogenation to MBA was comparatively low, allowing high yields to be achieved over all coatings. The difference was most obvious in the derivative plots, which show the reaction rates (Fig. 4g-i). Both Ce-titania supported

catalysts, especially Pd/Ti_{0.95}Ce_{0.05}O₂, showed high activity (Table 1). Pd/Ti_{0.95}Ce_{0.05}O₂ converted 2.6 times more MBY than Pd/TiO₂. Similar data were obtained in a batch reactor. The activity increases with an increase in the level of doping with cerium. At a Ce/Ti molar ratio of 0.2, the samples showed a reactivity 2.4 times higher than that of the undoped Pd/TiO₂ catalyst. The MBA formation rate at the initial reaction stage was significant over Pd/Ti_{0.95}Ce_{0.05}O₂ coating leading to a lower maximum MBE yield of 82.8 % in comparison to 90.1 % for the undoped Pd/TiO₂ coating. The derivative plots (Fig. 4g-i) demonstrate that with Zn adding the reaction rates decreased comparing Pd₈₀Zn₂₀/Ti_{0.95}Ce_{0.05}O₂ and Pd/Ti_{0.95}Ce_{0.05}O₂ coatings, which was expected considering the dilution of the Pd active sites by Zn. It is important that the MBA formation rate at the initial reaction stages was low, which makes it possible to achieve a maximum MBE yield of 89.0 %.

The effect of MBY concentration was studied in the range of 0.04-0.3 M over Pd/Ti_{0.95}Ce_{0.05}O₂, Pd₈₀Zn₂₀/Ti_{0.95}Ce_{0.05}O₂ and Pd/TiO₂ catalyst (Fig. 5). The initial MBY concentration insignificantly affects the hydrogenation rate over Pd/TiO₂ at an MBY concentration of 0.05-0.2 mol/L. The reaction order in MBY was 0.2. This is consistent with the literature data on the hydrogenation of alkyne [33,34]. The reaction order in MBY increased to 0.5 and 0.7 over Pd₈₀Zn₂₀/Ti_{0.95}Ce_{0.05}O₂ and Pd/Ti_{0.95}Ce_{0.05}O₂ coatings. After that, the effect of MBE concentration in the range of 0.05-0.3 M on the Pd/Ti_{0.95}Ce_{0.05}O₂ catalyst was studied. The catalyst was deactivated quickly within 3 runs and further deactivated within 4–10 runs. The rate of MBE hydrogenation in the first cycle was 15 times higher than in the third. Typical olefin catalytic hydrogensations occur not on pure metal surfaces but rather on surfaces covered with MBA formed as a result of MBE hydrogenation [35] or strongly bonded carbonaceous deposits that form immediately upon exposure to the reaction mixture such as alkylidyne adsorbed moieties [36].

The effect of reaction temperature and hydrogen partial pressure on conversion and selectivity was systematically studied over Pd₈₀Zn₂₀/Ti_{0.95}Ce_{0.05}O₂ and Pd/TiO₂. Selectivity tends to be slightly dependent on temperature. The MBE selectivity decreases over all coatings (Fig. 6a). The highest MBE yield was observed at 313 K. A decrease of activity was observed at a temperature above 328 K (Fig. 6b), which may be associated with the evaporation of methanol and a decrease in the partial pressure of hydrogen [10]. The apparent activation energy values for MBY hydrogenation calculated from Arrhenius plots derived from the data in Fig. 6b are 46, 51 and 63 kJ/mol over Pd/Ti_{0.95}Ce_{0.05}O₂, Pd₈₀Zn₂₀/Ti_{0.95}Ce_{0.05}O₂ and Pd/TiO₂, respectively. The apparent activation energy over Pd/TiO₂ is close to the previously reported value of 64 kJ/mol [8].

The reaction rate increased with increasing the hydrogen partial pressure from 0.28 to 1 in the whole range of temperatures studied (313–323 K). Our data presented in Fig. 7 confirmed that the

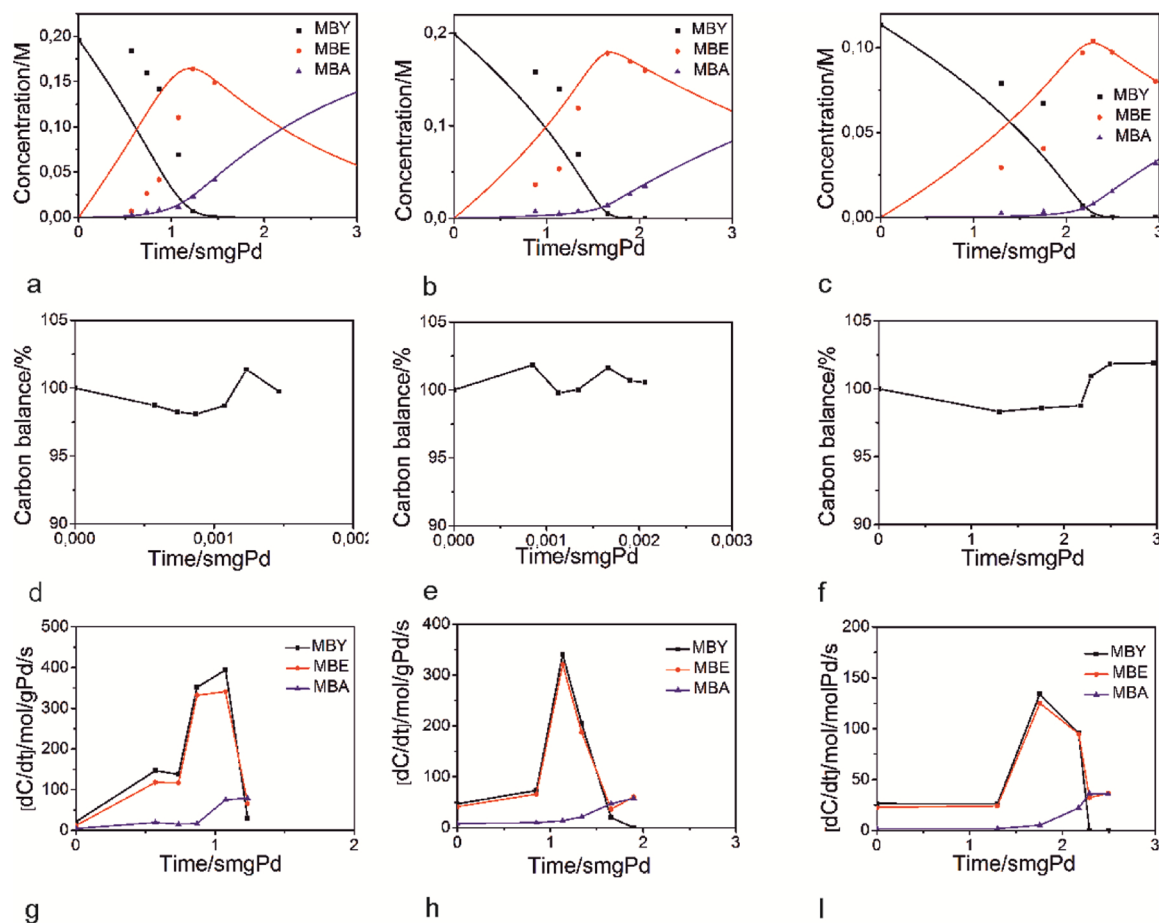


Fig. 4. Concentration profiles of MBY, MBE and MBA over Pd/Ti_{0.95}Ce_{0.05}O₂ (a), Pd₈₀Zn₂₀/Ti_{0.95}Ce_{0.05}O₂ (b) and Pd/TiO₂ (c) (the experimental data are shown by points, and the data from calculation by Langmuir–Hinshelwood model are shown by lines); carbon balances on Pd/Ti_{0.95}Ce_{0.05}O₂ (d), Pd₈₀Zn₂₀/Ti_{0.95}Ce_{0.05}O₂ (e) and Pd/TiO₂ (f), the apparent reaction rates on Pd/Ti_{0.95}Ce_{0.05}O₂ (g), Pd₈₀Zn₂₀/Ti_{0.95}Ce_{0.05}O₂ (h) and Pd/TiO₂ (i).

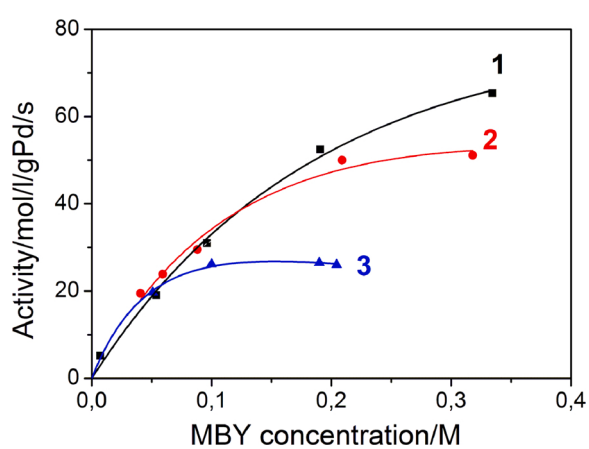


Fig. 5. Effect of the initial concentration of 2-methyl-3-butyn-2-ol on the activity at 20 % conversion in the hydrogenation of 2-methyl-3-butyn-2-ol over Pd/Ti_{0.95}Ce_{0.05}O₂ (1), Pd₈₀Zn₂₀/Ti_{0.95}Ce_{0.05}O₂ (2) and Pd/TiO₂ (3). v_g–2.00 mL/min, v_l–0.003–0.06 mL/min, MBY 0.05–0.32 M, pH₂ 1.0 atm, T 313 K.

hydrogenation of MBY shows a first order in hydrogen. (The hydrogen concentration (C_{H_2} 0.0135 mol/l) was calculated from the existing solubility data [37]). The first order can be attributed to the weaker hydrogen adsorption compared to the alkyne [33]. The rate-determining step is usually the addition of hydrogen to the adsorbed intermediate [38].

The concentration profiles of MBY hydrogenation at 0.5 atm of H₂ are presented in Fig. 8a–c. Activity at low hydrogen pressure decreased, which was expected considering the first order in hydrogen. In comparison with higher hydrogen pressure, the apparent MBA formation rate for the lower hydrogen pressure was slower. Varying liquid flow rate, selectivity versus conversion plots were constructed at a hydrogen pressure of 1 and 0.5 over Pd₈₀Zn₂₀/Ti_{0.95}Ce_{0.05}O₂ and Pd/TiO₂ (Fig. 9). The effect of hydrogen pressure depends on the catalyst composition. A decrease in the hydrogen pressure from 1 to 0.5 led to an increase in selectivity from 92.6% to 94.1% at 97% conversion over Pd₈₀Zn₂₀/Ti_{0.95}Ce_{0.05}O₂ (Fig. 9a). MBE selectivity over Pd/TiO₂ decreases from 92.6% to 91.7% at 98% conversion with decreasing hydrogen pressure from 1 to 0.5 (Fig. 9b).

4. Discussion

4.1. Kinetic model

MBY strongly adsorbs on the catalyst surface with subsequent hydrogenation (Fig. 10). The formed MBE (r_1) may fully hydrogenate to MBA after its adsorption (r_2) [39]. Direct MBY hydrogenation to MBA (r_3) may proceed via alkylidyne species [39]. A similar path has been proposed for the mechanism of acetylene [40,41] and pentyne [34] hydrogenation. It is known that catalysts are deactivated as a result of the absorption of the C₁₀-dimers near the Pd surface and, as a consequence, blocking of active centers [42]. In our experiments, we did not detect any dimer formation. High selectivity to MBE is expected when $r_2 + r_3 \ll r_1$, which refers to the extent to which MBA is formed from

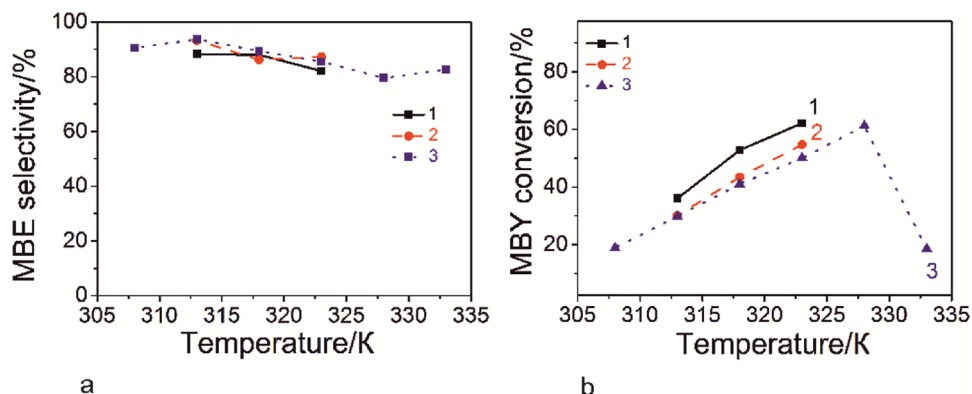


Fig. 6. Effect of temperature on MBE selectivity (a) and MBY conversion (b) over $\text{Pd}/\text{Ti}_{0.95}\text{Ce}_{0.05}\text{O}_2$ (1), $\text{Pd}_{80}\text{Zn}_{20}/\text{Ti}_{0.95}\text{Ce}_{0.05}\text{O}_2$ (2) and Pd/TiO_2 (3). MBY 0.2 M, v_g – 2.00 mL/min, H_2 1 atm, v_l – 0.02 mL/min (1, 2), v_l – 0.02 mL/min (3), T 313 K.

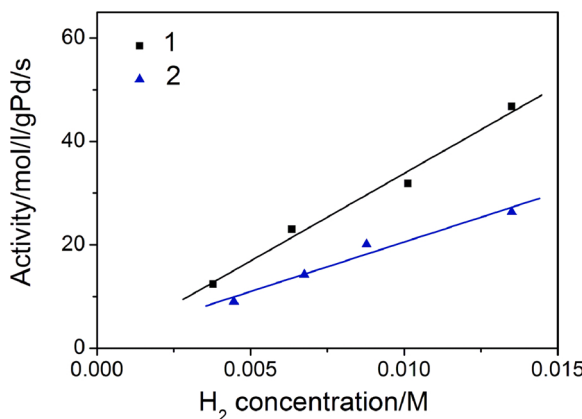


Fig. 7. Effect of the H_2 initial concentration on the activity at 20 % conversion in the hydrogenation of MBY over $\text{Pd}_{80}\text{Zn}_{20}/\text{Ti}_{0.95}\text{Ce}_{0.05}\text{O}_2$ (1) and Pd/TiO_2 (2). v_g – 2.00 mL/min, v_l – 0.003– 0.06 mL/min, MBY 0.1–0.2 M, H_2 0.28–1.0 at m., T 313 K.

MBY. When $K_{MBY} > K_{MBE}$, the surface is covered with alkyne, effectively preventing MBE from re-adsorption. MBE is fully hydrogenated (r_2) only at a very low MBY concentration (Fig. 2). The contribution of direct and sequential hydrogenation and, consequently, the selectivity of the catalyst are managed by the catalyst composition and the reaction conditions. Over hydrogenation on nonselective sites occurred over the surface with a bulk-dissolved metal hydride [43]. Palladium tends to form α - and β -hydrides, the latter decreasing the selectivity as it is responsible for the direct formation of the over hydrogenated product [42]. The formation of β -hydride is possible on catalysts containing cerium since the H_2 evolution from the $\beta\text{-PdH}_x$ phase was observed at 337 K in the TPR curve of the Pd/CeO_2 catalyst [44].

According to the low value of the Hatta number in capillary micro-reactors (<0.1), the catalytic reaction occurs in the kinetic regime [45]. Therefore, the kinetic equations can be applied without including mass transfer in the modeling. According to the experimentally obtained first order in hydrogen and fractional (noninteger) order with respect to MBY, two kinetic models can be assumed. The MBY consumption rate can be described by equations (1) (Model 1, Table 2) considering the following assumptions: (i) weak [38] and noncompetitive adsorption of hydrogen [8,45,46]. Another model 2 assumes that both MBY and H_2 are adsorbed on the catalyst and react with the formation of the adsorbed product at the Langmuir – Hinshelwood stage (competitive adsorption of the reactants takes place [19,47]). H_2 adsorption on Pd takes place via dissociation of the H–H bond [48]. There is a two-stage hydrogenation process: the first stage is quasi-equilibrium, and the addition of the second hydrogen atom is slow [38].

For the dependence of the rate on the initial concentrations of MBY (Fig. 5), kinetic modeling was carried out, assuming that only MBY is present on the surface ($K_{MBE}C_{MBE} \approx K_{MBA}C_{MBA} \ll K_{MBY}C_{MBY}$). The data were fitted using the Levenberg–Marquardt nonlinear least-squares algorithm. The calculated kinetic parameters of the possible models are presented in Table 3. The standard deviation of model 2 was the smallest, so this model was chosen for kinetic modeling. The calculation of the rate by model 2 is consistent with the experimental data (Fig. 4). It is noteworthy that the standard deviation is higher over Ce-doped coatings in comparison with undoped Pd/TiO_2 coating. It can be assumed that the increase in the standard deviation is caused by the assumption of identical adsorption constants for paths 1 and 3 and an increase in the rate constant of direct hydrogenation (k_3) for the samples doped with Ce.

4.2. Effect of Ce-doping of titania and Zn addition to nanoparticles

The support can affect the reactivity of the overlying nanoparticles in

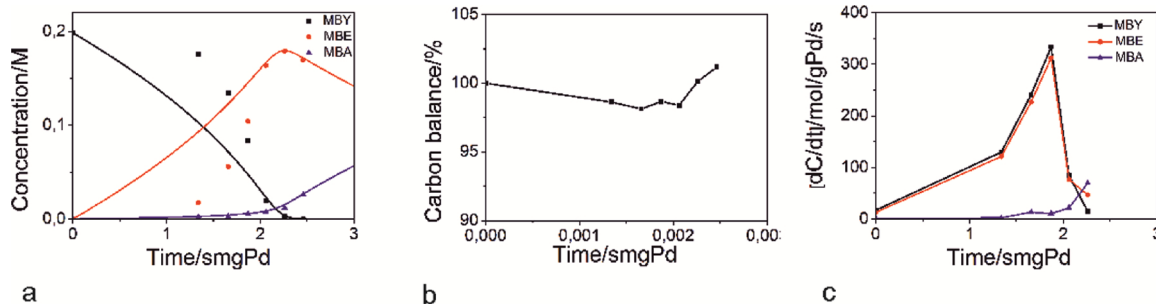


Fig. 8. Concentration profiles of MBY, MBE and MBA (a) over $\text{Pd}/\text{Ti}_{0.95}\text{Ce}_{0.05}\text{O}_2$ at hydrogen pressure 0.5 atm (the experimental data are shown by points, and the data from the calculation by Langmuir–Hinshelwood model are shown by lines); carbon balances (b), the apparent reaction rates (c).

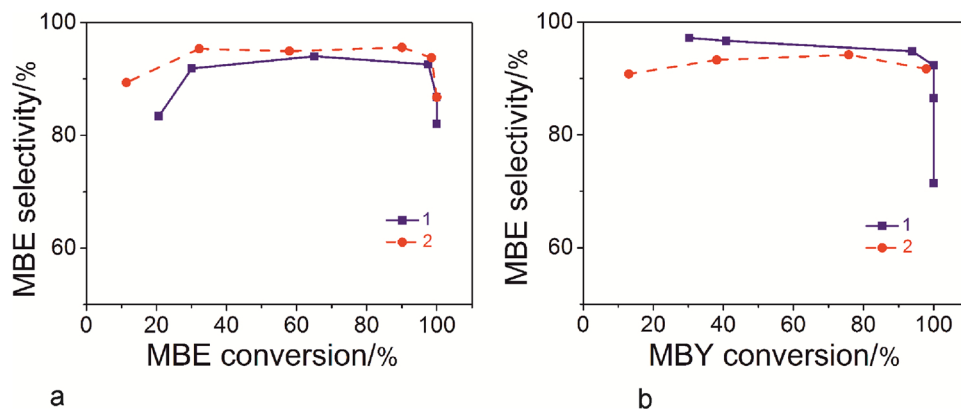


Fig. 9. MBE selectivity as a function of MBY conversion over $\text{Pd}_{80}\text{Zn}_{20}/\text{Ti}_{0.95}\text{Ce}_{0.05}\text{O}_2$ (a) and Pd/TiO_2 (b) at different hydrogen partial pressure. 1.0 atm H_2 (1); 0.5 atm H_2 (2). v_g – 2.00 mL/min, v_i – 0.020 mL/min, T 313 K, MBY 0.2 M (a), MBY 0.1 M (b).

2-methyl-3-butyn-2-ol 2-methyl-3-buten-2-ol 2-methyl-2-butanol

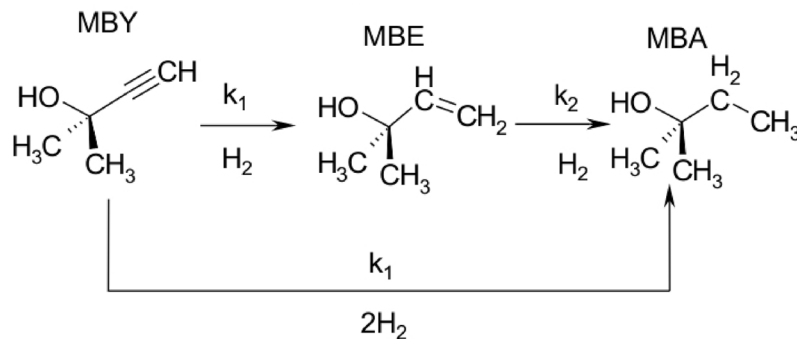


Fig. 10. Scheme of MBY hydrogenation.

several different ways: (1) by stabilizing the nanoparticles against coarsening [49], (2) by means of charge transfer to or from the nanoparticles (electronic interactions) [50–53] (3) by providing additional reaction sites [53] (4) by stabilizing intermediate reaction species [53, 54]. In general, it is impossible to predict which of these factors will dominate in heterogeneous catalytic reactions. Considerable attention should be paid to the support when a thorough understanding of the origin of the catalytic reactivity of the supported nanoparticles is desired. In the case of titania, strong metal-support interaction dramatically changes the catalytic performance [55].

The effects of Ce-doping and Zn adding were compared by studying the apparent reaction rates and the adsorption constants derived by kinetic modeling. The presented reaction rates have been integrated into Matlab using the ode45 function to solve systems of differential equations. The most common case in catalysis is the formation of non-equilibrium concentrations of active sites of the catalyst itself [56]. At high liquid flow rates and the beginning of the reaction, the catalyst surface is covered with chemisorbed hydrogen, there are few catalytic sites and the reaction rate is low. The system does not have time to reach equilibrium, therefore the estimation of the constants at <50 % conversion according to the Langmuir-Hinshelwood model is not correct. When modeling the kinetic curves with a longer exposure of the coating in the reaction mixture, the shape of the curve has changed, the initial reaction rate has increased, and the ratio of the constants has not changed. Solid lines in Figs. 4a–c and 8 a show the calculated concentration profiles that agree with the experimental data (within 12–23 % error), when the conversions are more than 50 % (Table 4). The resulting kinetic parameters obtained by the fitting are presented in Table 4. The K_{MBY} over the catalyst containing ceria is less than that over

the palladium supported on undoped titania. The K_{MBY} decreases in the following order: $\text{Pd}/\text{TiO}_2 > \text{Pd}_{80}\text{Zn}_{20}/\text{Ti}_{0.95}\text{Ce}_{0.05}\text{O}_2 > \text{Pd}/\text{Ti}_{0.95}\text{Ce}_{0.05}\text{O}_2$ (Table 3).

Results for activity in microcapillary reactors and batch reactors are shown in Table 1. The activity of the Ce-doped palladium samples is higher than that of the palladium supported catalyst without ceria. The difference is more pronounced with increasing Ce concentration. This may be explained by the occurrence of new catalytic centers due to the interaction of Pd-Ce which promotes MBY hydrogenation. We carried out XPS analysis and found that donation of electron density from Ce^{3+} to Pd is possible (in Supplementary SI1). Such donation can cause a change of the electronic state of the Pd surface and hence, a decrease of the adsorption strength of MBY. Borgna et al. [57] found that Cr addition to Pd increased the selectivity for partial hydrogenation of 1,3-butadiene. These results were attributed to charge transfer to the Pd4d band from Cr atoms, which was confirmed by XPS. Thus, in the presence of electron-donating additives of Ce^{3+} , surfaces show weak binding with alkyne (K_{MBY} in Table 4), enabling an increase in the rate of hydrogenation (k'_1 in Table 4) compared with the undoped support. The apparent rate constant k'_2 (Table 4) of MBE to MBA hydrogenation changed similarly to k'_1 constant, increasing for the Ce-doped one. Finally, another possibility is that the increase in activity is associated with the size of PdZn nanoparticles [58] and not with any interaction. We have recently shown that doping with Ce suppresses particle agglomeration during heat treatment due to the high thermal stability of the support [17]. However, our data on hydrogenation in a batch reactor show that the activity of powder catalysts doped with Ce constantly increases with increasing Ce concentration.

The surface of the catalyst is covered with alkyne up to almost 100 %

Table 2Kinetic models for MBY hydrogenation over Pd/Ti_{0.95}Ce_{0.05}O₂, Pd₈₀Zn₂₀/Ti_{0.95}Ce_{0.05}O₂, Pd/TiO₂ and rate expression for MBY consumption^a.

		Model 1
MBY + S	$\xrightleftharpoons{K_{MBY}} K_{MBY}$	$r_1 = k'_1 C_{MBY} K_{MBY} / (1 + K_{MBY} C_{MBY} + K_{MBE} C_{MBE} + K_{MBA} C_{MBA})$
MBE + S	$\xrightleftharpoons{K_{MBE}} K_{MBE}$	$r_2 = k'_2 C_{MBE} K_{MBE} / (1 + K_{MBY} C_{MBY} + K_{MBE} C_{MBE} + K_{MBA} C_{MBA})$
MBA + S	$\xrightleftharpoons{K_{MBA}} K_{MBA}$	$r_3 = k'_3 C_{MBA} K_{MBA} / (1 + K_{MBY} C_{MBY} + K_{MBE} C_{MBE} + K_{MBA} C_{MBA})$
H ₂ + S	$\xrightleftharpoons{k_{H2}} K_{H2}$	$k'_1 = k_1 K_{MBY} H_2 C_{Pd} C_{H2} \quad k'_2 = k_2 K_{MBE} H_2 C_{Pd} C_{H2}$ $k'_3 = k_3 K_{H2}^2 C_{Pd} C_{H2}^2$
MBYS + H ₂ S	$\xrightarrow{k_1} k_1$	$\frac{dC_{MBY}}{dt} = -(r_1 + r_3)$
MBES + H ₂ S	$\xrightarrow{k_2} k_2$	$\frac{dC_{MBE}}{dt} = r_1 - r_2$
MBYS + 2H ₂ S	$\xrightarrow{k_3} k_3$	$\frac{dC_{MBA}}{dt} = r_2 + r_3$
		Model 2
MBY + S	$\xrightleftharpoons{K_{MBY}} K_{MBY}$	$r_1 = k'_1 C_{MBY} K_{MBY} / (1 + K_{MBY} C_{MBY} + K_{MBE} C_{MBE} + K_{MBA} C_{MBA})^2$
MBE + S	$\xrightleftharpoons{K_{MBE}} K_{MBE}$	$r_2 = k'_2 C_{MBE} K_{MBE} / (1 + K_{MBY} C_{MBY} + K_{MBE} C_{MBE} + K_{MBA} C_{MBA})^2$
MBA + S	$\xrightleftharpoons{K_{MBA}} K_{MBA}$	$r_3 = k'_3 C_{MBA} K_{MBA} / (1 + K_{MBY} C_{MBY} + K_{MBE} C_{MBE} + K_{MBA} C_{MBA})^2$
H ₂ + 2S	$\xrightleftharpoons{k_{H2}} K_{H2}$	$k'_1 = k_1 K_{MBY} H_2 C_{Pd} C_{H2} \quad k'_2 = k_2 K_{MBE} H_2 C_{Pd} C_{H2}$ $k'_3 = k_3 K_{H2}^2 C_{Pd} C_{H2}^2$
MBYS + HS	$\xrightarrow{k_1} k_1$	$\frac{dC_{MBY}}{dt} = -(r_1 + r_3)$
MBYHS + S		
MBES + HS	$\xrightleftharpoons{k_2} k_2$	$\frac{dC_{MBE}}{dt} = r_1 - r_2$
MBEHS + S		
MBEHS + HS	$\xrightleftharpoons{k_3} k_3$	$\frac{dC_{MBA}}{dt} = r_2 + r_3$
MBYS + 4HS		
MBAS + 4S		

^a k_n is the rate constant for reaction n; K_{MBY} , K_{MBE} and K_{MBA} are the adsorption constants, and C_{MBY} , C_{MBE} and C_{MBA} , are the concentrations of alkyne, alkene, alkane, respectively.

Table 3

Kinetic parameters and standard deviation of model 1 and 2 calculated from dependence of the initial concentration of 2-methyl-3-butyn-2-ol on the activity at 20 % conversion.

N	Model	K/mol	k/mol/L/gPd/s	σ^a /mol/L/gPd/s
Pd/Ti _{0.95} Ce _{0.05} O ₂				
1	$kC_{MBY}/(1 + KC_{MBY})$	3.9 ± 0.7	117 ± 12	1.8
2	$kC_{MBY}/(1 + KC_{MBY})^2$	1.4 ± 0.2	302 ± 19	1.5
Pd ₈₀ Zn ₂₀ /Ti _{0.95} Ce _{0.05} O ₂				
1	$kC_{MBY}/(1 + KC_{MBY})$	8.5 ± 1.7	73 ± 6	2.2
2	$kC_{MBY}/(1 + KC_{MBY})^2$	2.5 ± 0.3	211 ± 9	1.8
Pd/TiO ₂				
1	$kC_{MBY}/(1 + KC_{MBY})$	44 ± 18	44 ± 2	1.3
2	$kC_{MBY}/(1 + KC_{MBY})^2$	6.5 ± 0.3	107 ± 1	0.4

^a Standard deviation.

conversion, which is caused by a 60 times higher MBY adsorption constant. Therefore, the MBE is not hydrogenated while MBY is present in the reaction mixture [8,19,32,35]. The selectivity of hydrogenation with respect to MBE, which is determined by the ratio $(r_1 + r_2)/(r_1 + r_3)$, over

Pd/Ti_{0.95}Ce_{0.05}O₂ is lower than that achieved over Pd/TiO₂ (Fig. 3). The Pd/Ti_{0.95}Ce_{0.05}O₂ coating doped with Ce showed the lowest ratio of the adsorption constants K_{MBY}/K_{MBE} (Table 4), and as a result, the lowest MBE selectivity. On the contrary, Zn adding increases the $(r_1 + r_2)/(r_1 + r_3)$ ratio from 86.3 % over the Pd/Ti_{0.95}Ce_{0.05}O₂ coating to 92.7 % over the Pd₈₀Zn₂₀/Ti_{0.95}Ce_{0.05}O₂ coating at 96 % conversion. The data obtained can be explained by the higher adsorption constant on bimetallic nanoparticles as compared to the palladium catalyst (Table 4). This result is in good agreement with previously reported data [7]. The PdZn phase was formed after the reduction at 523 K, which improves MBE selectivity [22]. On the one hand, Pd/TiO₂ has the highest MBY adsorption constant, and on the other hand, the k'_2 constant of MBE hydrogenation exceeds k'_1 constant of MBY hydrogenation (Table 4), which leads to low selectivity (Table 1). With a decrease in pressure, selectivity over Pd₈₀Zn₂₀/Ti_{0.95}Ce_{0.05}O₂ increased from 92.6% to 94.1% at a conversion of 97 % (Fig. 8a) and the alkyne adsorption constant also grew (Table 4). Several factors can affect the alkyne adsorption constant. Oxygen impurities in the added He can oxidize Pd [59], which leads to a decrease in the alkyne adsorption constant and selectivity, which was observed for Pd/TiO₂ coating (Fig. 9b). On the other hand part of Ce³⁺ is oxidized to Ce⁴⁺ causing a drop of alkyne adsorption constant (Table 4) and an increase in selectivity over Pd₈₀Zn₂₀/Ti_{0.95}Ce_{0.05}O₂ coating (Fig. 9a).

Table 4

Langmuir–Hinshelwood model parameters obtained by fitting the experimental data.

Catalyst	Pd/Ti _{0.95} Ce _{0.05} O ₂	Pd ₈₀ Zn ₂₀ /Ti _{0.95} Ce _{0.05} O ₂ ^a	Pd ₈₀ Zn ₂₀ /Ti _{0.95} Ce _{0.05} O ₂	Pd/TiO ₂
k'_1 /mol/L/gPd/s	796	586	687	303
k'_2 /mol/L/gPd/s	760	478	464	490
k'_3 /mol/L/gPd/s	5×10^{-6}	13	13	5×10^{-6}
K_{MBY} /L/mol	17	41	29	60
K_{MBE} /L/mol	1	1	1	1
K_{MBA} /L/mol	0.01	0.01	0.01	0.01
Maximum deviation/%	12	23	13	14
σ /mol/L	1.0×10^{-3}	1.4×10^{-3}	8.5×10^{-4}	1.1×10^{-3}

^a H₂ 0.5 atm.

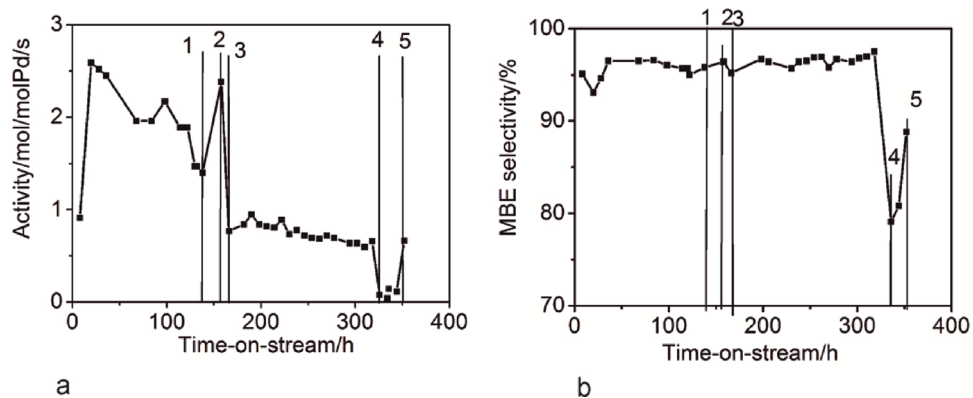


Fig. 11. Activity (a) conversion and MBE selectivity (b) at >97 % vs. time-on-stream over Pd₅₀Zn₅₀/Ti_{0.95}Ce_{0.05}O₂. v_g- 6.00 mL/min, v_I- 0.010- 0.040 mL/min, MBY 0.04–3.1 M pH₂ 1.0 atm, T 373 K.

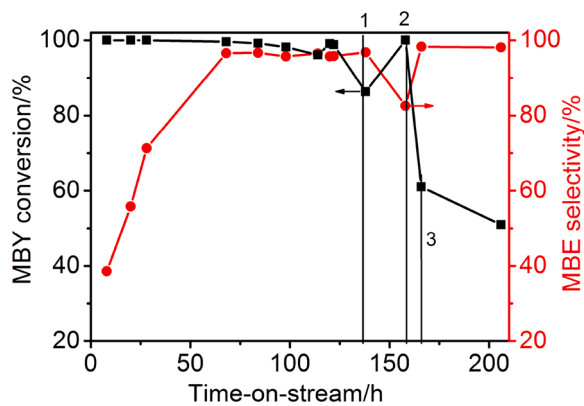


Fig. 12. MBY conversion and MBE selectivity over Pd₅₀Zn₅₀/Ti_{0.95}Ce_{0.05}O₂. v_g- 6.00 mL/min, v_I- 0.02 mL/min, MBY 1.0 M pH₂ 1.0 atm, T 373 K.

4.3. Coating stability and reuse

An important characteristic of the catalytic coating is its deactivation due to the leaching of metal and the support matrix. The long term stability of Pd₅₀Zn₅₀/Ti_{0.95}Ce_{0.05}O₂ coating was checked during 138 h

Table 5
Comparison of different coatings for MBY hydrogenation.

Coating	Reaction conditions	S ₉₈ /%	A/molMBY/molPd/s	Ref.
Pd ₂₅ Zn ₇₅ /TiO ₂	MBY 0.011 M, methanol, v _g - 1.0 mL/min, 1 atm of H ₂ , T 313 K.	89.5	0.04	[9]
Pd-Bi/TiO ₂	MBY 1.2 M, hexane, v _g - 10 mL/min, 1 atm of H ₂ , T 335 K.	93.0	0.21	[10]
Pd-Bi/TiO ₂	MBY 10 M, v _g - 10 mL/min, 1 atm of H ₂ , T 303 K.	93.0	1.6	[12]
Pd/ZnO	MBY 10 M, v _g - 10 mL/min, 1 atm of H ₂ , T 343 K.	97.5 ^a	0.8	[11,61]
Pd/ZnO/Al ₂ O ₃	MBY 10 M, v _g - 0.7 L/min, 4 atm of H ₂ , v _I - 1.4 L/min, T 333 K.	83	0.003	[46]
Pd/SiO ₂	MBY 6 M, v _g - 0.5 L/min, 4 atm of H ₂ , v _I - 0.045 L/min, T 373 K.	91	1.3	[62]
Pd ₅₀ Zn ₅₀ / (Ti _{0.95} Ce _{0.05}) O ₂	MBY 1 M, methanol, v _I - 0.02 mL/min v _g - 6.00 mL/min, 1 atm of H ₂ , T 313 K, 68 h on stream	96.5	2.5	Current work

^a MBY conversion 85 %.

on stream in terms of activity and selectivity at >97 % conversion (Fig. 11) and conversion and selectivity at a constant liquid flow rate (Fig. 12). Our results showed that the MBY (1.0 M) conversion increases from 36.6 % to 99.4 % at a liquid flow rate of 0.03 mL/min during 20 h on stream due to cleaning the active surface from carbonaceous deposits [22]. Increasing run time from 20 h to 68 h increased selectivity from 93.5 % to 96.5 % at nearly 100 % conversion (Fig. 11b). The best MBE yield of 95.8 % at 99 % conversion was obtained after 68 h on stream (Fig. 11a). The Pd₅₀Zn₅₀/Ti_{0.95}Ce_{0.05}O₂ coating exhibited better activity and selectivity in comparison with reported earlier (Table 5), so high liquid product yields can be achieved and there is a large potential for realization of this technology on an industrial scale. Constant MBE selectivity of 96–97 % was observed in the next 70 h of operation (Fig. 12). MBY conversion decreased from 100 to 83 % during 138 h on stream. A negative result of metal leaching was obtained when analyzing the resulting product solution after 138 h on stream which is consistent with previous research [60]. Since the deactivation rate was found to be 8 % of the initial activity per day (Fig. 11a), the hydrogenation reaction was performed over the Pd₅₀Zn₅₀/Ti_{0.95}Ce_{0.05}O₂-2 reduced in hydrogen at 573 K for 2 h after 138 h on stream (Fig. 13). Reduction recovered the initial activity of the catalyst. Thus, it can be concluded that the decrease in activity in the period from 20 to 138 h on stream can be explained by the destruction of the active center as a result of the Ce³⁺ - Ce⁴⁺ oxidation. Calcination at 573 K (treatment 3) did not affect selectivity to MBE (Figs. 12 and 13), decreased activity by 2.8 times (Fig. 13) and reduced conversion from 100 % to 61 % (Fig. 12). Within the next 152 h activity gradually decreased from 0.77 to 0.66 mol/molPd/s (Fig. 11a), and selectivity remained constant

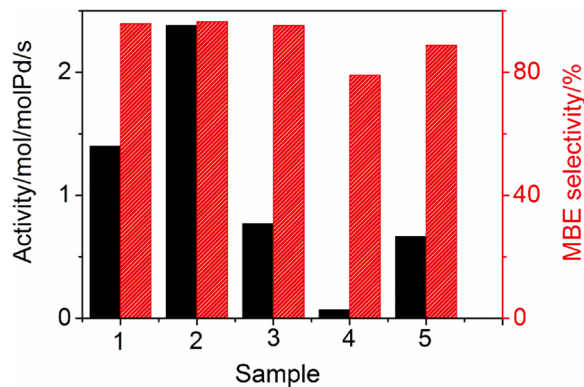


Fig. 13. Effect of activation conditions on the activity and selectivity at 97 % conversion in hydrogenation of 2-methyl-3-butyn-2-ol over Pd/Ti_{0.95}Ce_{0.05}O₂. v_g- 6.00 mL/min, v_I- 0.0025- 0.020 mL/min, MBY 0.12 M, pH₂ 1.0 atm, T 313 K.

(Figs. 11b and 12), the MBY conversion decreased from 61 to 51 % during 40 h on stream (Fig. 12). Calcination at higher temperature 673 K (treatment 4), increased MBA formation, attaining 76 % selectivity, which is restored to 88 % after reduction in H₂ at 573 K for 2 h (treatment 5) (Fig. 13). The lower activity after oxidation-reduction treatment can be associated with the sintering of nanoparticles and oxidation of Pd. TEM data indicate an increase in particle size from 3 to 9–19 nm (in Supplementary SI2). XPS spectra of the Pd_{3d} level in the Pd₅₀Zn₅₀/Ti_{0.95}Ce_{0.05}O₂-4 show a peak at high BE_s, which can be attributed to Pd²⁺ (Supplementary SI2). Consequently, the structure of the active center of PdZn underwent changes upon calcination due to oxidation of Pd, which led to a weakening of the bond with alkyne [59]. ICP-AES analysis of the acid-dissolved coating (aqua regia) showed that the Pd content decreased from 1.30 (excluding polymer residues) to 0.69 wt.% at a constant Pd/Zn molar after 352 h on stream. Thus, it can be concluded that the decrease in activity was also caused by the leaching of Pd during hydrogenation reactions, which was caused by the segregation and oxidation of nanoparticles [12].

5. Conclusions

The support and nanoparticle compositions affect strongly the activity and selectivity of the catalytic coatings inside the capillary reactor in the selective hydrogenation of MBY. In contrast to the catalysts used in a traditional batch reactor including the commercial Lindlar catalyst, these coatings are suitable for a continuous microcapillary reactor, and they exceed the examples described in the literature in terms of activity and selectivity. Three catalysts were superior in one of the above parameters: Pd/Ti_{0.95}Ce_{0.05}O₂ for activity, Pd/TiO₂ for selectivity, Pd₈₀Zn₂₀/Ti_{0.95}Ce_{0.05}O₂ exhibits high activity, selectivity and stability. A kinetic model was proposed that describes well the kinetics of MBY hydrogenation. Test duration and redox treatments significantly affect the properties of catalytic coatings. The activity decreases and the selectivity increases with an increase in the reaction time from 20 to 138 h. Reduction in H₂ at 573 K for 2 h restores the activity of Pd₅₀Zn₅₀/Ti_{0.95}Ce_{0.05}O₂, while oxidation at >573 K and subsequent reduction at 573 K leads to irreversible decline of catalytic properties.

CRediT authorship contribution statement

Lyudmila B. Okhlopkova: Conceptualization, Methodology, Data curation, Validation, Writing - original draft. **Igor P. Prosvirin:** Visualization, Investigation, Software. **Mikhail A. Kerzhentsev:** Writing - review & editing. **Zinfer R. Ismagilov:** Supervision, Project administration.

Declaration of Competing Interest

The authors report no declarations of interest.

Acknowledgements

Authors are grateful to Dr. E.Yu. Gerasimov for investigation of the catalysts by TEM. This work was supported by the Federal Agency for Scientific Organizations (project no. 0303-2016-0004).

This work was conducted within the framework of budget project (project no. 0303-2016-0004) for Boreskov Institute of Catalysis.

Appendix A. Supplementary data

Supplementary material related to this article can be found, in the online version, at doi:<https://doi.org/10.1016/j.cep.2020.108240>.

References

- [1] W. Bonrath, M. Eggersdorfer, T. Netscher, Catalysis in the industrial preparation of vitamins and nutraceuticals, *Catal. Today* 121 (2007) 45–57, <https://doi.org/10.1016/j.cattod.2006.11.021>.
- [2] G. Biardi, G. Baldi, Three-phase catalytic reactors, *Catal. Today* 52 (1999) 223–234, [https://doi.org/10.1016/S0920-5861\(99\)00077-2](https://doi.org/10.1016/S0920-5861(99)00077-2).
- [3] C.B. Minnich, L. Greiner, C. Reimers, M. Uerdingen, M.A. Liauw, Bridging the gap: a nested-pipe reactor for slow reactions in continuous flow chemical synthesis, *Chem. Eng. J.* 168 (2011) 759–764, <https://doi.org/10.1016/j.cej.2010.09.004>.
- [4] W. Ehrfeld, V. Hessel, H. Löwe, *Microreactors: New Technology for Modern Chemistry*, Wiley-VCH Verlag, Weinheim, 2000.
- [5] A. Pashkova, L. Greiner, Towards small-scale continuous chemical production: technology gaps and challenges, *Chem. Ing. Tech.* 83 (2011) 1337–1342, <https://doi.org/10.1002/cite.201100037>.
- [6] V. Hessel, D. Kralisch, N. Kockmann, T. Noël, Q. Wang, Novel process windows for enabling, accelerating, and uplifting flow chemistry, *ChemSusChem* 6 (2013) 746–789, <https://doi.org/10.1002/cssc.201200766>.
- [7] D.M. Roberge, L. Ducry, N. Bieler, P. Cretton, B. Zimmermann, Microreactor technology: a revolution for the fine chemical and pharmaceutical industries? *Chem. Eng. Technol.* 28 (2005) 318–323, <https://doi.org/10.1002/ceat.200407128>.
- [8] E.V. Rebrov, E.A. Klinger, A. Berenguer-Murcia, E.M. Sulman, J.C. Schouten, Selective hydrogenation of 2-methyl-3-butyne-2-ol in a wall-coated capillary microreactor with a Pd₂₅Zn₇₅/TiO₂ catalyst, *Org. Process Res. Dev.* 13 (2009) 991–998, <https://doi.org/10.1021/op900085b>.
- [9] E.V. Rebrov, A. Berenguer-Murcia, H.E. Skelton, B.F.G. Johnson, A.E.H. Wheatley, J.C. Schouten, Capillary microreactors wall-coated with mesoporous titania thin film catalyst supports, *Lab Chip* 9 (2009) 503–506, <https://doi.org/10.1039/B815716B>.
- [10] N. Cherkasov, A.O. Ihbadon, E.V. Rebrov, Novel synthesis of thick wall coatings of titania supported Bi poisoned Pd catalysts and application in selective hydrogenation of acetylene alcohols in capillary microreactors, *Lab Chip* 15 (2015) 1952–1960, <https://doi.org/10.1039/C4LC01066C>.
- [11] N. Cherkasov, M. 'moun Al-Rawashdeh, A.O. Ihbadon, E.V. Rebrov, Scale up study of capillary microreactors in solvent-free semihydrogenation of 2-methyl-3-butyn-2-ol, *Catal. Today* 273 (2016) 205–212, <https://doi.org/10.1016/j.cattod.2016.03.028>.
- [12] N. Cherkasov, A.O. Ihbadon, E.V. Rebrov, Solvent-free semihydrogenation of acetylene alcohols in a capillary reactor coated with a Pd-Bi/TiO₂ catalyst, *Appl. Catal. A Gen.* 515 (2016) 108–115, <https://doi.org/10.1016/j.apcata.2016.01.019>.
- [13] O. Muraza, E.V. Rebrov, M.H.J.M. de Croon, J.C. Schouten, Enhancement of the stability of microporous silica films in non-aqueous solvents at elevated temperature, *Microporous Mesoporous Mater.* 124 (2009) 20–29.
- [14] D.Z.G. Li, J.C. Yu, Thermally stable ordered mesoporous CeO₂/TiO₂ visible-light photocatalysts, *Phys. Chem. Chem. Phys.* 11 (2009) 3775–3782.
- [15] Y. Zhang, A.H. Yuwono, J. Wang, J. Li, Enhanced photocatalysis by doping cerium into mesoporous titania thin films, *J. Phys. Chem. C* 113 (2009) 21406–21412, <https://doi.org/10.1021/jp907901k>.
- [16] M. Martos, B. Julián-López, J.V. Folgado, E. Cordoncillo, P. Escrivano, Sol-gel synthesis of tunable cerium titanate materials, *Eur. J. Inorg. Chem.* 2008 (2008) 3163–3171, <https://doi.org/10.1002/ejic.2008000303>.
- [17] L.B. Okhlopkova, M.A. Kerzhentsev, Z.R. Ismagilov, Improved thermal stability of PdZn/TiO₂coating by Ce doping, *Surf. Eng.* 31 (2015) 78–83, <https://doi.org/10.1179/1743294414Y.0000000408>.
- [18] A. Yarulin, I. Yuranov, F. Cárdenas-Lizana, P. Abdulkhan, L. Kiwi-Minsker, Size-effect of Pd-(poly(N-vinyl-2-pyrrolidone)) nanocatalysts on selective hydrogenation of alkynes with different alkyl chains, *J. Phys. Chem. C* 117 (2013) 13424–13434, <https://doi.org/10.1021/jp402258s>.
- [19] N. Semagina, M. Grasemann, N. Xanthopoulos, A. Renken, L. Kiwi-Minsker, Structured catalyst of Pd/Zn on sintered metal fibers for 2-methyl-3-butyn-2-ol selective hydrogenation, *J. Catal.* 251 (2007) 213–222, <https://doi.org/10.1016/j.jcat.2007.06.028>.
- [20] M.J. Maccarrone, C.R. Lederhos, G. Torres, C. Betti, F. Coloma-Pascual, M. E. Quiroga, Partial hydrogenation of 3-hexyne over low-loaded palladium mono and bimetallic catalysts, *Appl. Catal. A* 441–442 (2012) 90–98.
- [21] L. Shen, S. Mao, J. Li, M. Li, P. Chen, H. Li, Z. Chen, Y. Wang, PdZn intermetallic on a CN@ZnO hybrid as an efficient catalyst for the semihydrogenation of alkynes, *J. Catal.* 350 (2017) 13–20, <https://doi.org/10.1016/j.jcat.2017.01.021>.
- [22] L.B. Okhlopkova, S.V. Cherepanova, I.P. Prosvirin, M.A. Kerzhentsev, Z. R. Ismagilov, Semi-hydrogenation of 2-methyl-3-butyn-2-ol on Pd-Zn nanoalloys prepared by polyol method: effect of composition and heterogenization, *No Title, Appl. Catal. A* 549 (2018) 245–253.
- [23] L.B. Okhlopkova, E.V. Matus, I.P. Prosvirin, M.A. Kerzhentsev, Z.R. Ismagilov, Selective hydrogenation of 2-methyl-3-butyn-2-ol catalyzed by embedded polymer-protected PdZn nanoparticles, *J. Nanopart. Res.* 17 (2015) 1–15, <https://doi.org/10.1007/s11051-015-3289-6>.
- [24] Trajan Scientific and Medical, (2020). https://www.trajanscimed.com/products/pdpn-1085-g?_pos=1&_sid=0a5c1804d&_ss=r.
- [25] Agilent, (2020). <https://www.agilent.com/store/productDetail.jsp?catalogId=1602530-10>.
- [26] L.B. Okhlopkova, M.A. Kerzhentsev, F.V. Tuzikov, Y.V. Larichev, Z.R. Ismagilov, Palladium-zinc catalysts on mesoporous titania prepared by colloid synthesis. II. Synthesis and characterization of PdZn/TiO₂ coating on inner surface of fused silica capillary, *J. Nanopart. Res.* 14 (2012) 1–15, <https://doi.org/10.1007/s11051-012-1088-x>.

- [27] L.B. Okhlopkova, E.V. Matus, I.Z. Ismagilov, M.A. Kerzhentsev, Z.R. Ismagilov, Synthesis of nanosized thin-film bimetallic catalysts based on mesoporous TiO₂ for microstructured reactors, *Kinet. Catal.* 54 (2013) 511–519, <https://doi.org/10.1134/S0023158413040162>.
- [28] S. Dominguez-Dominguez, A. Berenguer-Murcia, D. Cazorla-Amoros, A. Linares-Solano, Semihydrogenation of phenylacetylene catalyzed by metallic nanoparticles containing noble metals, *J. Catal.* 243 (2006) 74–81, <https://doi.org/10.1016/j.jcat.2006.06.027>.
- [29] L.B. Okhlopkova, E.V. Matus, I.Z. Ismagilov, M.A. Kerzhentsev, I.P. Prosvirin, Z. R. Ismagilov, Synthesis of mesoporous bimetallic Pt-Sn catalytic coatings from polynuclear precursors for fine organic synthesis processes, *J. Struct. Chem.* 54 (2013), <https://doi.org/10.1134/S0022476613060061>.
- [30] M.K. Akbar, D.A. Plummer, S.M. Ghiaasiaan, On gas-liquid two-phase flow regimes in microchannels, *Int. J. Multiph. Flow* 29 (2003) 855–865, [https://doi.org/10.1016/S0301-9322\(03\)00043-0](https://doi.org/10.1016/S0301-9322(03)00043-0).
- [31] D. Chisholm, A theoretical basis for the Lockhart-Martinelli correlation for two-phase flow, *Int. J. Heat Mass Transf.* 10 (1967) 1767–1778, [https://doi.org/10.1016/0017-9310\(67\)90047-6](https://doi.org/10.1016/0017-9310(67)90047-6).
- [32] L.Z. Nikoshvili, A.S. Makarova, N.A. Lyubimova, A.V. Bykov, A.I. Sidorov, I. Y. Tyamina, V.G. Matveeva, E.M. Sulman, Kinetic study of selective hydrogenation of 2-methyl-3-butyn-2-ol over Pd-containing hypercrosslinked polystyrene, *Catal. Today* 256 (2015) 231–240, <https://doi.org/10.1016/j.cattod.2015.02.033>.
- [33] G.C. Bond, *Metal-Catalysed Reactions of Hydrocarbons*, Springer, 2005.
- [34] M.W. Tew, M. Janousch, T. Huthwelker, J.A. van Bokhoven, The roles of carbide and hydride in oxide-supported palladium nanoparticles for alkyne hydrogenation, *J. Catal.* 283 (2011) 45–54, <https://doi.org/10.1016/j.jcat.2011.06.025>.
- [35] N. Cherkasov, A.O. Ibadon, A.J. McCue, J.A. Anderson, S.K. Johnston, Palladium-bismuth intermetallic and surface-poisoned catalysts for the semi-hydrogenation of 2-methyl-3-butyn-2-ol, *Appl. Catal. A Gen.* 497 (2015) 22–30, <https://doi.org/10.1016/j.apcata.2015.02.038>.
- [36] F. Zaera, Key unanswered questions about the mechanism of olefin hydrogenation catalysis by transition-metal surfaces: a surface-science perspective, *Phys. Chem. Chem. Phys.* 15 (2013) 11988–12003.
- [37] C. Descamps, C. Coquelet, C. Bouallou, D. Richon, Solubility of hydrogen in methanol at temperatures from 248.41 to 308.20 K, *Thermochim. Acta* 430 (2005) 1–7, <https://doi.org/10.1016/j.tca.2004.12.001>.
- [38] U.K. Singh, M.A. Vannice, Liquid-phase citral hydrogenation over SiO₂-supported group VIII metals, *J. Catal.* 199 (2001) 73–84, <https://doi.org/10.1006/jcat.2000.3157>.
- [39] S. Leviness, V. Nair, A.H. Weiss, Z. Schay, L. Guczi, Acetylene hydrogenation selectivity control on PdCu/Al₂O₃ catalysts, *J. Mol. Catal.* 25 (1984) 131–140.
- [40] A.N.R. Bos, K.R. Westerterp, Mechanism and kinetics of the selective hydrogenation of ethyne and ethene, *Chem. Eng. Process. Process Intensif.* 32 (1993) 1–7, [https://doi.org/10.1016/0255-2701\(93\)87001-B](https://doi.org/10.1016/0255-2701(93)87001-B).
- [41] A.S. Al-Ammar, G. Webb, Hydrogenation of acetylene over supported metal catalysts. Part 3.—[14C]tracer studies of the effects of added ethylene and carbon monoxide on the reaction catalysed by silica-supported palladium, rhodium and iridium, *J. Chem. Soc. Faraday Trans. 1 Phys. Chem. Condens. Phases* 75 (1979) 1900, <https://doi.org/10.1039/f19797501900>.
- [42] M.A. Aramendia, V. Borau, C. Jimenez, J.M. Marinas, M.E. Sempere, F.J. Urbano, Optimization of the selective semi-hydrogenation of phenylacetylene with supported palladium systems, *Appl. Catal.* 63 (1990) 375–389.
- [43] W. Palczewska, Catalytic reactivity of hydrogen on palladium and nickel hydride phases, *Adv. Catal.* (1975) 245–291, [https://doi.org/10.1016/S0360-0564\(08\)60484-8](https://doi.org/10.1016/S0360-0564(08)60484-8).
- [44] Z. Zhan, X. Liu, H. He, L. Song, J. Li, D. Ma, Fabrication of a flower-like Pd/CeO₂ material with improved three-way catalytic performance, *J. Rare Earths* 31 (2013) 750–758, [https://doi.org/10.1016/S1002-0721\(12\)60353-6](https://doi.org/10.1016/S1002-0721(12)60353-6).
- [45] L.N. Protasova, E.V. Rebrov, H.E. Skelton, A.E.H. Wheatley, J.C. Schouten, A kinetic study of the liquid-phase hydrogenation of citral on Au/TiO₂ and Pt-Sn/TiO₂ thin films in capillary microreactors, *Appl. Catal. A Gen.* 399 (2011) 12–21, <https://doi.org/10.1016/j.apcata.2011.03.021>.
- [46] S. Vernuccio, R. Goy, P. Rudolf Von Rohr, J. Medlock, W. Bonrath, Hydrogenation of 2-methyl-3-butyn-2-ol over a Pd/ZnO catalyst: kinetic model and selectivity study, *React. Chem. Eng.* 1 (2016) 445–453, <https://doi.org/10.1039/c6re00093b>.
- [47] N. Semagina, E. Joannet, S. Parra, E. Sulman, A. Renken, L. Kiwi-Minsker, Palladium nanoparticles stabilized in block-copolymer micelles for highly selective 2-butyne-1,4-diol partial hydrogenation, *Appl. Catal. A Gen.* 280 (2005) 141–147, <https://doi.org/10.1016/j.apcata.2004.10.049>.
- [48] H.F. Busnengo, C. Crespos, W. Dong, A. Salin, J.C. Rayez, Role of orientational forces in nonactivated molecular dissociation on a metal surface, *Phys. Rev. B - Condens. Matter Mater. Phys.* 63 (2001) 414021–414024, <https://doi.org/10.1103/physrevb.63.041402>.
- [49] J.H. Kang, E.W. Shin, W.J. Kim, J.D. Park, S.H. Moon, Selective hydrogenation of acetylene on Pd/SiO₂ catalysts promoted with Ti, Nb and Ce oxides, *Catal. Today* 63 (2000) 183–188, [https://doi.org/10.1016/S0920-5861\(00\)00458-2](https://doi.org/10.1016/S0920-5861(00)00458-2).
- [50] W.W. Lonergan, T. Wang, D.G. Vlachos, J.G. Chen, Effect of oxide support surface area on hydrogenation activity: Pt/Ni bimetallic catalysts supported on low and high surface area Al₂O₃ and ZrO₂, *Appl. Catal. A Gen.* 408 (2011) 87–95, <https://doi.org/10.1016/j.apcata.2011.09.007>.
- [51] S. Bhogeswararao, D. Srinivas, Intramolecular selective hydrogenation of cinnamaldehyde over CeO₂-ZrO₂-supported Pt catalysts, *J. Catal.* 285 (2012) 31–40, <https://doi.org/10.1016/j.jcat.2011.09.006>.
- [52] K. Choe, F. Zheng, H. Wang, Y. Yuan, W. Zhao, G. Xue, X. Qiu, M. Ri, X. Shi, Y. Wang, G. Li, Z. Tang, Fast and selective semihydrogenation of alkynes by palladium nanoparticles sandwiched in metal-organic frameworks, *Angew. Chem. - Int. Ed.* 59 (2020) 3650–3657, <https://doi.org/10.1002/anie.201913453>.
- [53] J. Serrano-Ruiz, J. Luetich, A. Sepulveda-Escribano, F. Rodriguez-Reinoso, Effect of the support composition on the vapor-phase hydrogenation of crotonaldehyde over Pt/Ce_xZr_{1-x}O₂ catalysts, *J. Catal.* 241 (2006) 45–55, <https://doi.org/10.1016/j.jcat.2006.04.006>.
- [54] R. de S. Monteiro, F.B. Noronha, L.C. Dieguez, M. Schmal, Characterization of PdCeO₂ interaction on alumina support and hydrogenation of 1,3-butadiene, *Appl. Catal. A Gen.* 131 (1995) 89–106, [https://doi.org/10.1016/0926-860X\(95\)00137-9](https://doi.org/10.1016/0926-860X(95)00137-9).
- [55] S.J. Tauster, S.C. Fung, R.L. Garten, Strong metal-support interactions. Group 8 noble metals supported on titanium dioxide, *J. Am. Chem. Soc.* 100 (1978) 170–175, <https://doi.org/10.1021/ja00469a029>.
- [56] Heterogeneous catalysis, in: F.G. Helfferich (Ed.), *Compr. Chem. Kinet.*, 2004, pp. 273–308, [https://doi.org/10.1016/S0069-8040\(04\)80013-X](https://doi.org/10.1016/S0069-8040(04)80013-X). Chapter 9.
- [57] A. Borgna, New supported palladium-chromium catalysts: characterization and catalytic properties, *J. Catal.* 128 (1991) 99–112, [https://doi.org/10.1016/0021-9517\(91\)90070-K](https://doi.org/10.1016/0021-9517(91)90070-K).
- [58] N. Semagina, A. Renken, D. Laub, L.L. Kiwi-Minsker, Synthesis of monodispersed palladium nanoparticles to study structure sensitivity of solvent-free selective hydrogenation of 2-methyl-3-butyn-2-ol, *J. Catal.* 246 (2007) 308–314, <https://doi.org/10.1016/j.jcat.2006.12.011>.
- [59] L.B. Okhlopkova, M.A. Kerzhentsev, Z.R. Ismagilov, Internal surface coating of a capillary microreactor for the selective hydrogenation of 2-methyl-3-butyn-2-ol over PdZn/TiO₂ catalyst. The effect of the catalyst's activation conditions on its catalytic properties, *Kinet. Catal.* 59 (2018) 347–356, <https://doi.org/10.1134/S0023158418030163>.
- [60] E.V. Rebrov, E.A. Klinger, A. Berenguer-Murcia, E.M. Sulman, J.C. Schouten, Selective hydrogenation of 2-methyl-3-butyn-2-ol in a wall-coated capillary microreactor with a Pd25Zn75/TiO₂ catalyst, *Org. Process Res. Dev.* 13 (2009) 991–998, <https://doi.org/10.1021/op900085b>.
- [61] N. Cherkasov, P. Denissenko, S. Deshmukh, E.V. Rebrov, Gas-liquid hydrogenation in continuous flow – the effect of mass transfer and residence time in powder packed-bed and catalyst-coated reactors, *Chem. Eng. J.* 379 (2020) 122292, <https://doi.org/10.1016/j.cej.2019.122292>.
- [62] M. Kundra, B. Bin Mohamad Sultan, D. Ng, Y. Wang, D.L.J. Alexander, X. Nguyen, Z. Xie, C.H. Hornung, Continuous flow semi-hydrogenation of alkynes using 3D printed catalytic static mixers, *Chem. Eng. Process. - Process Intensif.* 154 (2020) 108018, <https://doi.org/10.1016/j.cep.2020.108018>.